Supplement

A. Details of a quantitative stability analysis by using Poincaré point correlations

Qualitatively, Figures 2, 6 and 7 shown in our article seem to favour the RK method: The structure of the time-dependent dynamics of the RK exponents is simpler than the one of the established Oseledec method. Hence, it seems worthwhile to quantitatively compare both methods. There are ways to test the complexity of their local exponents, see Chlouverakis et al. [S1]. However, the local exponents themselves are merely tools to analyse the chaos of a given nonlinear dynamics. The question is therefore rather: How well are the given trajectories assessed by the local exponents? How well are the exponents correlated to the trajectories? How can the degree of the associated complexity be evaluated? Here we discuss an approach similar to an established method to compare the volatility of financial values is constructed, namely the evaluation of the standard deviation of the distribution of the values.

A.1 Description of the Poincaré point correlated deviation

It seems sufficient to analyse only a typical set of points in a reduced *n-1* dimensional subspace. For Lorenz chaos, an *xy*-plane will be defined by *z*=constant, see Fig. S1. Pairs of neighbours of the points in this plane are selected and their distance r is evaluated. Then, the absolute difference $\Delta\lambda$ of the corresponding local exponents is evaluated as a function of the distance r of these neighbouring points i,k.

$$\Delta\lambda_{ik}(r) = \left| \lambda_i - \lambda_k \right| \qquad \text{with} \quad r^2 = (x_i\text{-}x_k)^2 + (y_i\text{-}y_k)^2 \tag{S1}$$

Finally, plots of the strictly local exponents are compared to the exponents of the $\boldsymbol{V}$ and $\boldsymbol{W}$ frames which incorporate integrals over previous times. This comparison can be performed in a quantitative way and results in a measure of how well the $\boldsymbol{V}$ and $\boldsymbol{W}$ frames correspond to the trajectories to be analysed. The strength of chaotic behaviour is manifest in the 'pseudo'-irregularity of the differences $\Delta\lambda_{ik}(r)$, which is measurable by its standard deviation, after a possible underlying regular behaviour has been eliminated (we call it 'pseudo'-irregular, since all data points are regularly determined by eq. (1), including the rotations of the frames).

The following quantitative procedure will be used to evaluate the distribution of the data depending on the function $\Delta\lambda_{ik}(r<r_m)$ up to radius r_m. Since there might be a systematic bias as a function of r, it seems appropriate to first get rid of this bias. Therefore, the values $\Delta\lambda_{ik}(r)$ are fitted by a linear approximation resulting in $a_{ik}(r)$ for each point ik. Then the standard deviation Q of the resulting difference $[\Delta\lambda_{ik}(r) - a_{ik}(r)]$ is considered to be an adequate measure for the correlation of the exponent λ with the trajectories, called here 'Poincaré point correlated deviation' (PPCD),

$$Q_{\mathrm{PPCD}}(\lambda) = \mathrm{std}\,[\Delta\lambda_{ik}(r) - a_{ik}(r)] \qquad \text{(S2)}$$

The quantity $Q_{\mathrm{PPCD}}(\lambda_{local})$ of the strictly local exponents serves as a basis to assess the strength of the chaos of the trajectory. Then, $Q_{\mathrm{PPCD}}(\lambda_{V\text{-frame}})$ and $Q_{\mathrm{PPCD}}(\lambda_{W\text{-frame}})$ are compared to $Q_{\mathrm{PPCD}}(\lambda_{local})$. The resulting fractions f_V and f_V analyse quantitatively the correlation of both frames with the trajectories,

$$f_V = Q_{\mathrm{PPCD}}(\lambda_{V\text{-frame}}) \;/\; Q_{\mathrm{PPCD}}(\lambda_{local}) \qquad \text{(S3)}$$

$$f_W = Q_{\mathrm{PPCD}}(\lambda_{W\text{-frame}}) \;/\; Q_{\mathrm{PPCD}}(\lambda_{local}) \;. \qquad \text{(S4)}$$

If $f_{\mathrm{frame}} >> 1$, the respective frame adds chaotic behaviour to the complexity of the trajectories, which has to be eliminated by long-time integration. For $f_{\mathrm{frame}} \approx 1$, this frame could also be used to analyse short portions of different chaotic transients.

A.2 Poincaré point correlated deviations' for Lorenz chaos

A.2.1 A peculiar structure of the points in the Poincaré plane

For Lorenz chaos, fixing z=40 defines an *xy*-plane, which serves for finding Poincaré points where trajectories cross the plane. Such Poincaré points $p(t)$ have already been used for the previous 'Poincaré integrals', defined in terms of time limits between consecutive points for decreasing z-values. Here, both points $p^{(+)}(t)$ and $p^{(-)}(t)$ for increasing and decreasing z, respectively, are evaluated. However, in addition to the times t_i also the positions x_i,y_i are considered. A plot of these Poincaré points in the Poincaré *xy*-plane reveals a particular structure, see Fig. S2 (top): There are two branches of $p^{(-)}$ points around the centre, one

with y>x, denoted by c1, and the other with $y<x$, denoted by c2. The $p^{(+)}$ points have branches on the left (ℓ) torus and on the right (r) torus. Each branch consists of a narrow band of points with only a small scattering around a smooth curve. It is now straightforward to determine for each point $p^{(-)}(t_i)$ if the corresponding trajectory comes from ℓ or r and goes to ℓ or r by analysing the time series $p^{(+)}(t_{i-1})$, $p^{(-)}(t_i)$, $p^{(+)}(t_{i+1})$. The result is striking: the points c1 display only the sequences ℓ→ℓ or ℓ→r plotted in Fig. A2 (bottom) as circles ○ and x signs, respectively. Moreover, these two possibilities are separated in the Poincaré plane. Similarly, the c2 points consist only of an r→r or r→ℓ sequences, plotted as stars * and + signs, respectively. This symmetry allows restricting the analysis to the c1 branch.

At this point an interesting question can be asked: Where on the trajectory could additional noise most easily change the dynamical behaviour? As an example, perturb the trajectory at z=40 where the ℓ→ℓ sequence is close to the ℓ→r sequence, thus the circles ○ and x are very close, such that the trajectory jumps from one to the other sequence. At this position a noise-induced transition as described by Gassmann [S2] would be most easily possible

To provide an overview, the local exponents of the c1 points are plotted as a function of the x component in Fig. S3. The separation between the ℓ→ℓ and ℓ→r sequences is marked by a vertical line. The strictly local exponents are: extreme expansion α_1 (top left), extreme orthogonal divergence β_1 (top right). The second exponent $\lambda_{\parallel W}$ of the $\boldsymbol{W}$ frame of local acceleration is also a strictly local exponent (bottom right). The central row displays the first exponents λ_{V1} and $\lambda_{\perp W}$, the bottom row the second exponents λ_{V2} and $\lambda_{\parallel W}$ of the $\boldsymbol{V}$ frame (left) and of the $\boldsymbol{W}$ frame (right), respectively. It is interesting that all three plots on the right side (extreme orthogonal divergence β_1 and $\boldsymbol{W}$ frame) share the same feature: The values of the exponents all differ for the two sequences, the barrier is marked by a horizontal line indicating a complete correlation to the behaviour of remaining on the same left loop, or changing the loop, which certainly implies a larger divergence. This feature is missing for both exponents of the $\boldsymbol{V}$ frame (left centre and left bottom) showing a large spreading.

A.2.2 Poincaré point correlated deviation analysis of Lorenz chaos

For each point of the c1 branch all local exponents are stored. Then the distance to neighbouring points is evaluated and registered for the radius $r<r_{max}$=0.4, together with the absolute difference $|\Delta\lambda_{ik}(r)|$ of the corresponding local exponents λ. These values are plotted as functions of r in Fig. S3, arranged similarly to

Fig. S2. The pairs *ik* between ℓ→ℓ points are depicted as circles ○, pairs between ℓ→r as x symbol and the rare pairs between ℓ→ℓ and ℓ→r as stars *. The straight lines in Fig. S4 represent linear approximations to the data points. Only the differences of the acceleration $|\Delta\lambda_{\parallel W}|$ (bottom right) exhibit a distinct bias as a function of the radius *r*, due to the strong dependence of these local exponents along the branch c1, as seen for $\lambda_{\parallel W}$ in Fig. S3 (bottom right). Clearly, all plots of Fig. S4 show a strongly irregular pattern of the data. However, the magnitude of this spread is very different, see the corresponding scales, resulting in the following $Q_{\mathrm{PPCD}}(\lambda)$ values: left, from top to bottom: 0.013, 1.8, 1.8, and right, from top to bottom: 0.017, 0.015, 0.022. The average for the three strictly local exponents (0.013, 0.017, 0.022) is 0.017. The average of the two ***V*** exponents is 1.8, and the only ***W*** exponent $|\Delta\lambda_{\perp W}|$ subject to integration (centre right) has a value of 0.015. Therefore, the quantitative factors *f* defined by eqs. (S3) and (S4) are

$$f_V \approx 100 \qquad \text{(S5)}$$

$$f_W \approx 1 \quad . \qquad \text{(S6)}$$

resulting in a 'figure of merit' f_W / f_V of around 1:100 in favour of RK.

Although the heuristic PPCD analysis provides a strong oversimplification by using only a small selected portion of the data, its outcome is surprisingly clear. In order to visualize this final result, Fig. S4 is potted again as Fig. S5, but now with the same scale for all plots. Obviously, only the Oseledec ***V*** frame (left centre and bottom) is adding a strong chaotic complexity to the complexity of the trajectories to be analyzed.

B. Local extreme divergence in the phase space $R\{\underline{x}\}$ independent from trajectories

In this section we further refine the local stability analysis of Section 6 in our article. Since the 'constrained' exponent $\beta_{\perp 1}$ of true divergence is only a function of the position $\underline{x}$ in the phase space and does, therefore, not depend on a trajectory, its value can be evaluated directly in the full phase space $R\{\underline{x}\}$. These values are shown in Fig. S6 as a mesh plot for the *xy* plane at *z* values 60 (top left) and 20 (bottom left). The strange Lorenz attractor is about along the diagonal $x \approx y$ where the values $\beta_{\perp 1}$ are low, but with a higher pass between the sections of the two loops. A *yz*-plot of the trajectory for this analysis is found in Fig. S1 of Section A above..

A simple local indicator of the curvature of trajectories in the phase space can be found easily: For the evaluation of the local acceleration, the new vector $\boldsymbol{J}\,f_{\|}$ after the time interval dt is projected by the scalar product $(f_{\|}\cdot \boldsymbol{J}\,f_{\|})$ onto the flow direction $f_{\|}$. The absolute magnitude of the new vector minus the absolute magnitude of the projection is a measure for the deviation at t+dt from the direction $f_{\|}$ at t of the local trajectory and hence a measure of the curvature of the trajectory,

$$d = \left|\boldsymbol{J}\,f_{\|}\right| - \left|(f_{\|}\cdot \boldsymbol{J}\,f_{\|})\right| \qquad \text{(S7)}$$

This 'deviation' d is shown in Fig. S6 on the right side. In more detail, the Jacobian matrix $\boldsymbol{J}$ can be written as a sum of a symmetric matrix $\boldsymbol{S}$ and an anti-symmetric $\boldsymbol{D}$: $\boldsymbol{J}=\boldsymbol{S}+\boldsymbol{D}$. The evaluated separate action of these matrices onto d reveals a very different behaviour: The symmetric $\boldsymbol{S}$ causes a strongly varying peculiar pattern in the region of the strange attractor, but its action is nearly negligible outside the attractor. In contrast, the anti-symmetric $\boldsymbol{D}$ creates a rather smooth structure, small at the attractor, but increasingly large with larger distance from the attractor. The combined action of these different sources are visible in Fig. S6 on the right side as a varying peculiar pattern along the diagonal ($\boldsymbol{S}$), and smooth increase outside ($\boldsymbol{D}$).

C. Are local exponents norm-independent?

Local Lyapunov exponents are based on ratios of distances between points in phase space and their relative angles in order to discriminate between rotation and elongation, measured in the metric of the coordinate system chosen. Only transformations which do not change these ratios and/or relative angles locally leave the exponents unchanged. Examples are orthogonal rotations of Cartesians or equally enlarging all distances without changing angles. However, nonlinear transformations might change the local exponents. Even an unequal scaling of a Cartesian changes exponents corresponding to directions with components of unequally spaced coordinates, see the example of the scaled harmonic oscillator in [S3]. In 1993, H.R. Moser et al. [S4] already noted that a nonlinear change of the metric for a polar angle θ_i from cos θ_i to θ_i in the Hamiltonian of nonlinear ferromagnetic resonance phenomena [S5] destroys the sign-symmetry of the local exponents if the damping term is neglected. Earlier in 1990 W.G. Hoover et al. [S6] displayed different distributions of exponents for Cartesian and polar coordinates. Since the directions of all frames used the

same algorithm to find the corresponding exponents, all frames are only norm-independent for rather trivial coordinate transformations.

Although local exponents are by definition not universal, for practical use this problem is easily overcome by using the same coordinate system with the same metric for comparing local instabilities under parameter change in the equations of motion.

References

[S1] K.E. Chlouverakis, A. Argyris, A. Bogris, and D. Syvridis, Complexity and synchronization in chaotic fiber-optic systems, Physica D 237 (2008) 568-572, and references therein.

[S2] F. Gassmann, Noise-induced chaos-order transitions, Phys. Rev. E 55 (1997) 2215-2221.

[S3] H. Bosetti, H.A. Posch, C. Dellago and W.G. Hoover, Time-reversal symmetry and covariant Lyapunov vectors for simple particle models in and out of thermal equilibrium, arXiv:1004.4473 (The scaled oscillator is not in ref. [16] of our article).

[S4] H.R. Moser , P.F. Meier, F. Waldner, Numeric simulations of chaotic and hyperchaotic signals measured in nonlinear magnetic resonance, Phys. Rev. B 47 (1993) 217-226.

[S5] F. Waldner, A 'stroboscopic model' for nonlinear ferromagnetic resonance phenomena, J. Phys. C: Solid State Phys. 21, (1988) 1243-1255.

[S6] Wm.G. Hoover, C.G. Hoover, H.A. Posch, Lyapunov instability of pendulums, chains, and strings, Phys. Rev. A 41 (1990) 2999-3004.

Figure Captions

Fig. S1. Lorenz model with control parameters (σ, ρ, b)=(16, 40, 4). Trajectories are projected onto the *yz* plane at equal time intervals to indicate the changes in velocity. The line indicates the position of the Poincaré planes $z=c_p$=const. with c_p=40 Local exponents are integrated over each time interval between consecutive Poincaré points.

Fig. S2. Lorenz chaos: *xy* plot of Poincaré points at z=40. Top: all points. Bottom: blow up of the central sections for decreasing z values. Upper left branch c1: symbol o denotes the sequence ℓ→ℓ(left torus), symbol + denotes the sequence ℓ→r(right torus). Lower right branch c2: * for r→r and x for r→ℓ.

Fig. S3. Lorenz chaos: Local exponents of c1 points ℓ→ℓ (o) and ℓ→r (+) of Fig. A2 vs. the x component. Vertical lines separate o from +. Left: top extreme expansion α_i, centre λ_{V1}, bottom λ_{V2}. Right: top extreme orthogonal expansion $\beta_{\perp 1}$, centre $\lambda_{\perp W1}$, bottom $\lambda_{\parallel W} = \varphi_{\parallel}$. Horizontal lines separate values of o from +.

Fig. S4. Lorenz chaos, PPCD analysis: Absolute difference $|\Delta\lambda_{ik}(r)|$ of the corresponding local exponents λ vs. radius $r<r_{max}=0.4$ of pairs ik between ℓ→ℓ , denoted by the symbol o, between ℓ→r , denoted by +, and the rare pairs between ℓ→ℓ and ℓ→r , denoted by *. Lines: linear approximations of the data points. The differences are of the same exponents as plotted in Fig. S3.

Fig. S5. Lorenz chaos: The same PPCD data points as shown in Fig. S4, but all plotted on the same scale to indicate the differences of the magnitude of the V frame (left centre and bottom) to the W frame (right centre) and to the strictly local exponents.

Fig. S6. Lorenz chaos: The 'constrained' exponent $\beta_{\perp 1}$ of true separation is only a function of the position $\underline{x}$ (independent of any trajectory) in the phase space $R\{\underline{x}\}$. Its values are plotted as a mesh on an xy plane at z values 60 (top) and 20 (bottom) on the left side. The local measure d, eq. (S7), of the curvature along the trajectory through $\underline{x}$ is plotted on the right side for the same z values.

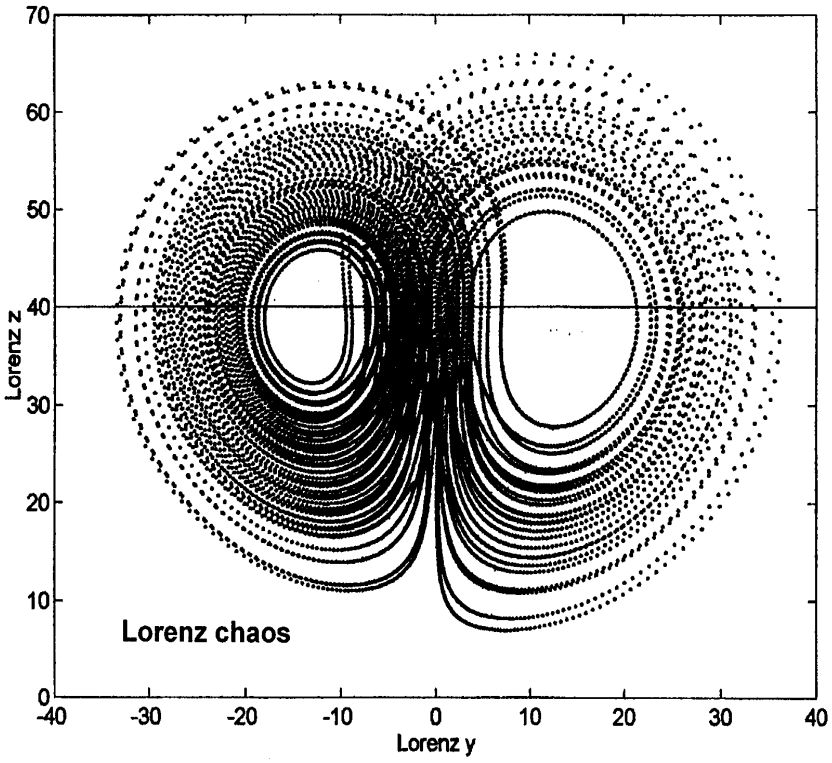
Lorenz chaos
Lorenz z
Lorenz y
70
60
50
40
30
20
10
0
-40
-30
-20
-10
0
10
20
30
40

Fig. S1

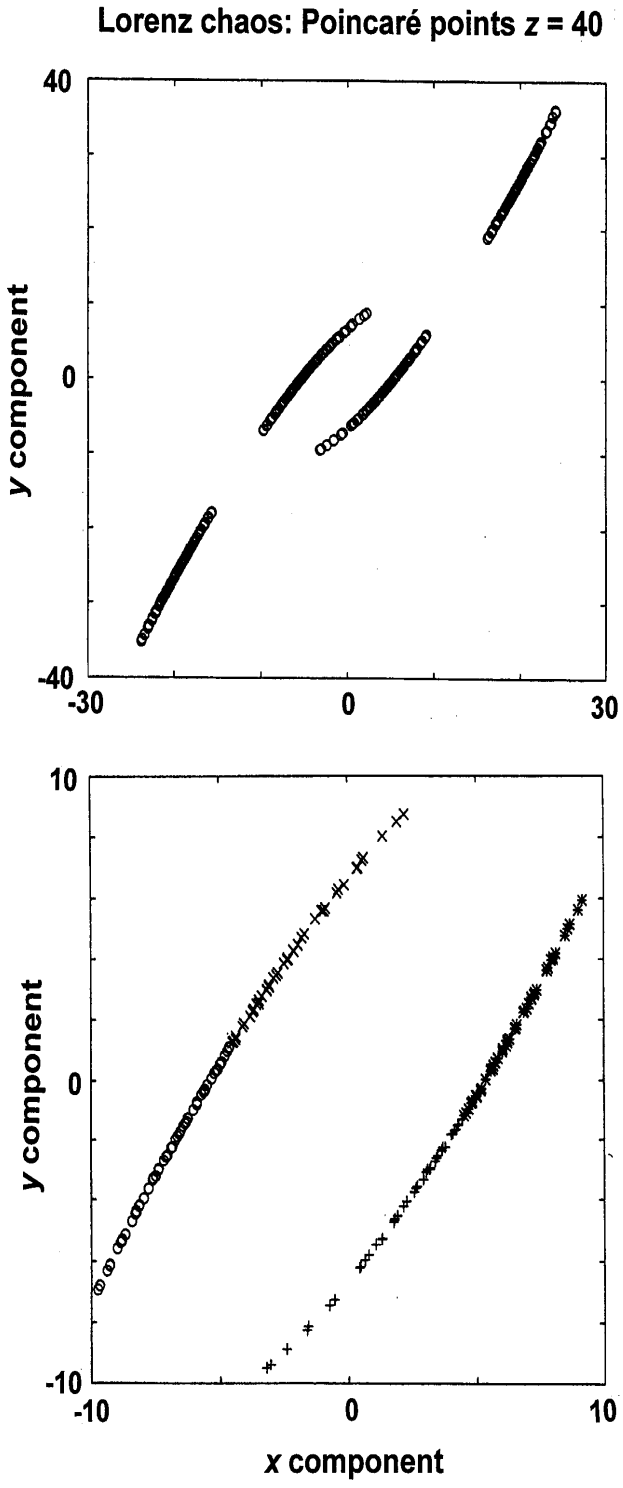
Lorenz chaos: Poincaré points z = 40
40
0
-40
-30
0
30
y component
10
0
-10
-10
0
10
y component
x component

Fig. S2

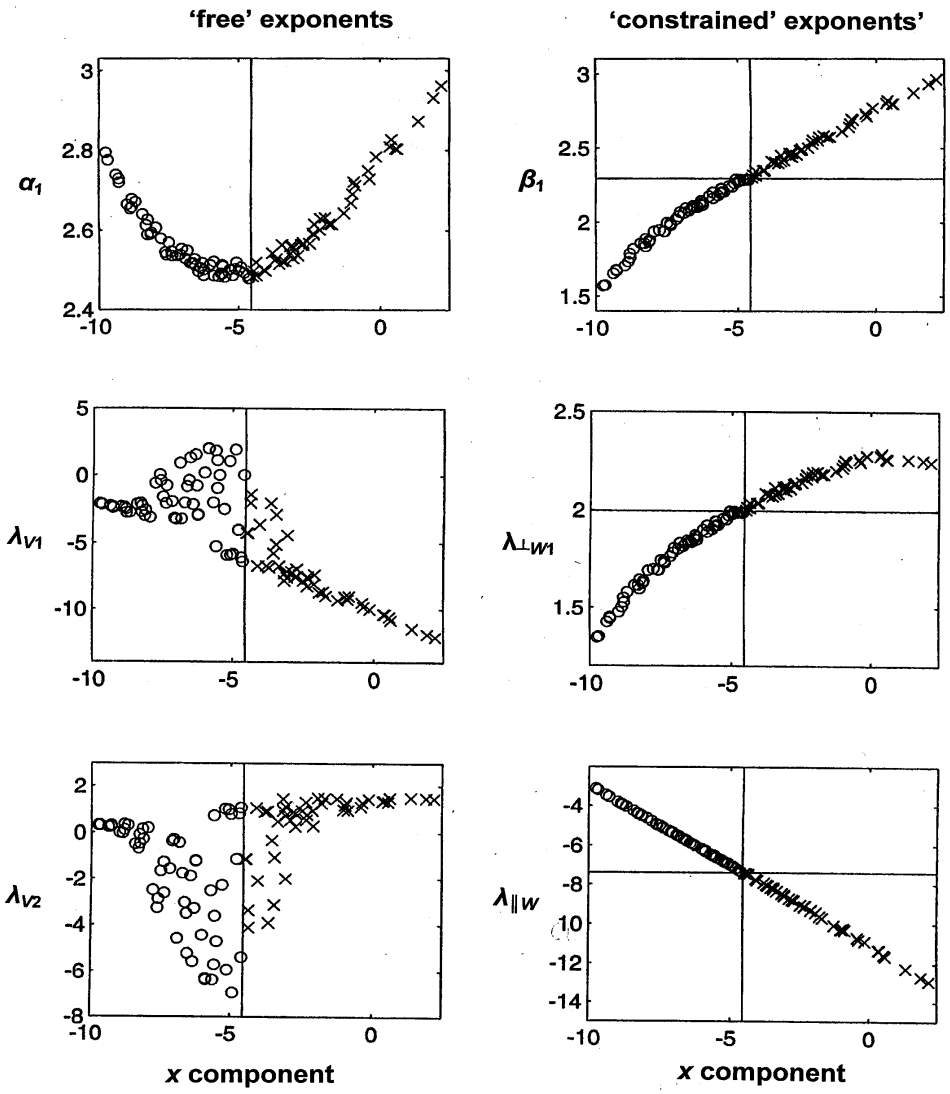
'free' exponents
'constrained' exponents'
α_1
β_1
λ_{V1}
$\lambda_{\perp W1}$
λ_{V2}
$\lambda_{\parallel W}$
x component
x component

Fig. S3

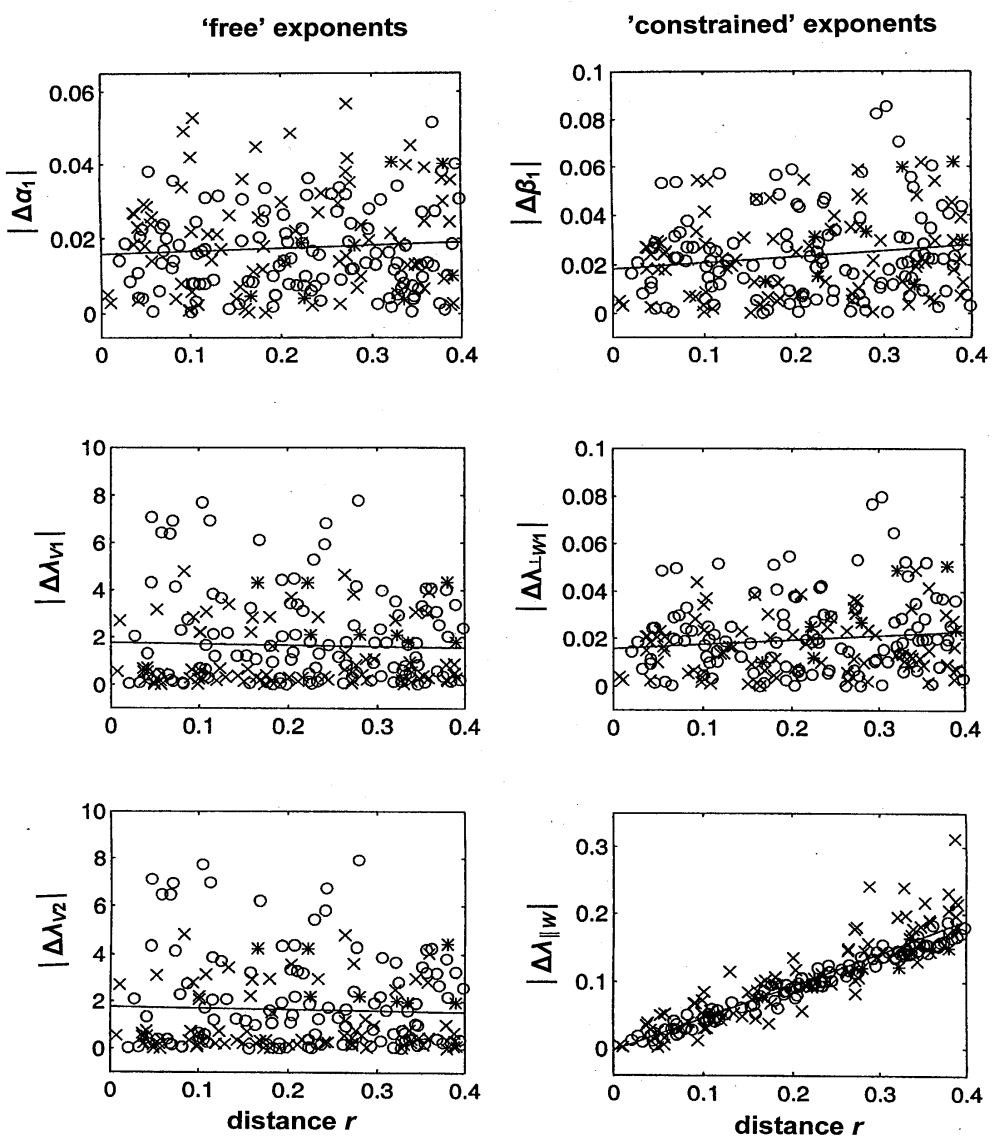
'free' exponents
'constrained' exponents
$|\Delta\alpha_1|$
$|\Delta\beta_1|$
$|\Delta\lambda_{V1}|$
$|\Delta\lambda_{LW1}|$
$|\Delta\lambda_{V2}|$
$|\Delta\lambda_{\|W}|$
distance r
distance r

Fig. S4

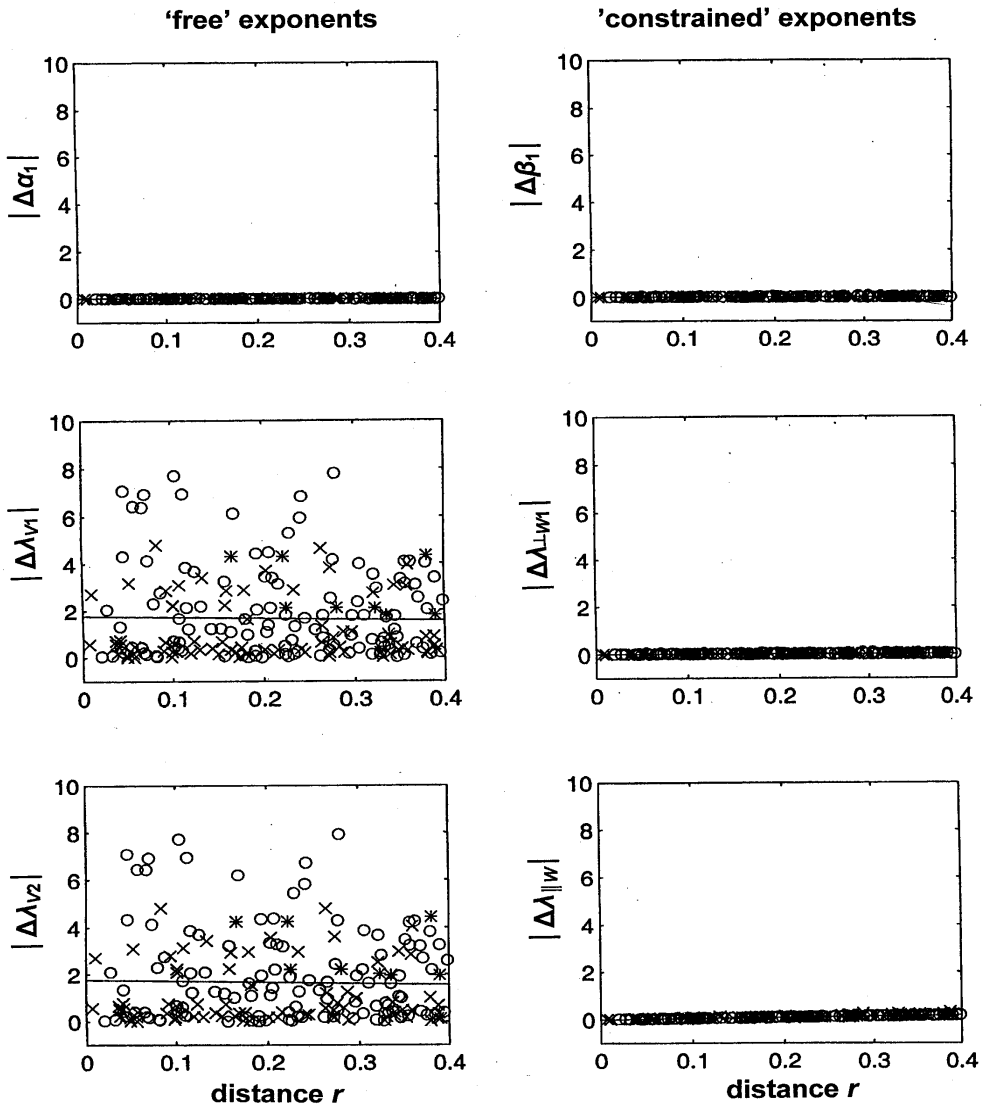
'free' exponents
'constrained' exponents
$|\Delta\alpha_1|$
$|\Delta\beta_1|$
$|\Delta\lambda_{V1}|$
$|\Delta\lambda_{LW1}|$
$|\Delta\lambda_{V2}|$
$|\Delta\lambda_{\|W}|$
distance r
distance r

Fig. S5

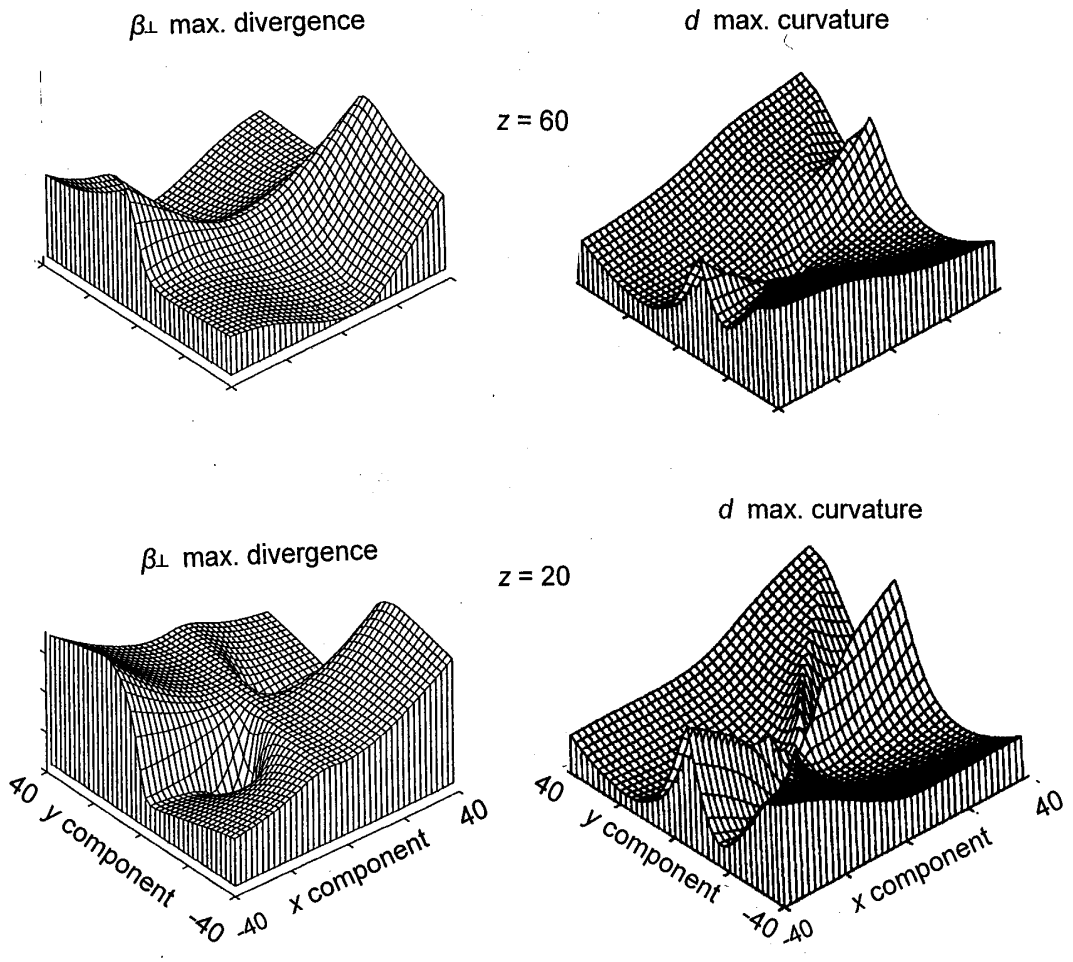
β⊥ max. divergence
d max. curvature
z = 60
β⊥ max. divergence
d max. curvature
z = 20
40
y component
-40
-40
x component
40
40
y component
-40
-40
x component
40

Fig. S6